

## Pressure-induced structural transformations in cadmium selenide nanorods

Nicholas Jabari Lee, Rajiv K. Kalia, Aiichiro Nakano, and Priya Vashishta<sup>a)</sup>  
*Collaboratory for Advanced Computing and Simulations, Department of Chemical Engineering  
 and Materials Science, Department of Physics and Astronomy, and Department of Computer Science,  
 University of Southern California, Los Angeles, California 90089-0242*

(Received 2 May 2006; accepted 28 June 2006; published online 28 August 2006)

Pressure induced structural transformations in cadmium selenide (CdSe) nanorods are studied using parallel molecular dynamics. Nanorods (4.4 nm in diameter and 4.4 to 53 nm in length) are embedded in a liquid and subjected to pressure. Reversible structural transformations are observed from wurtzite to a single domain rocksalt crystal phase. The simulation results reveal a decrease in transformation pressure with rod length. The transformation mechanism involves atomic shifts within the (0001) plane of the wurtzite structure and is similar to the one observed in electronic structure calculations of pressure-induced structural transformation in bulk CdSe. © 2006 American Institute of Physics. [DOI: 10.1063/1.2338808]

Pressure-induced structural phase transitions in nanoscale systems have been an exciting area of research since the early 1980s.<sup>1–5</sup> The mechanical and structural properties of nanoparticles have been shown in theory and experiment to determine or influence their optical and electronic properties.<sup>6</sup> Thus, understanding the mechanisms governing structural transformations at the nanoscale can help bring about future developments in nano-materials and devices.<sup>7,8</sup> Recent efforts have focused on pressure-driven structural phase transitions from four-fold coordinated zinc blende to six-fold coordinated rocksalt (RS) phase in GaAs and other semiconductors. Electronic structure calculations based on the density-functional theory (DFT) and molecular dynamics simulations have been used to confirm pathways and barriers between pressure-induced zinc blende to rocksalt transformations.<sup>9,10</sup> Transformation mechanisms from four-fold wurtzite (WZ) to six-fold RS coordinated structures in Cadmium selenide (CdSe), are also of considerable interest. The Alivisatos group has studied CdSe nanorod ensembles under cyclic pressure in experiments<sup>11–13</sup> and observed reversible transformations between four-coordinated and six-coordinated crystal phases. Single domain formation was observed in shorter rods while multiple domain formation was seen in longer rods. Despite a great deal of interest and activity in this area, the transformation mechanism for wurtzite to rocksalt transformation in CdSe at nanoscale is not well understood.<sup>14–18</sup>

In this letter, we report the results of molecular dynamics (MD) simulations of CdSe nanorods of varying lengths undergoing forward and reverse structural phase transformation under hydrostatic pressure, infer the pathways for the structural transformation, and report the observation of structural phase transformation pressure dependence on nanorod length.

Four sets of simulations are performed on single nanorods. Each nanorod has a diameter of 44 Å—approximately the diameter of the nanorods in Alivisato's experiments. The width-to-length ratios of the nanorods are 1:1, 1:2, 1:4, and 1:12. We refer to each simulation by nanorod aspect ratio—

$S_{1:1}$ ,  $S_{1:2}$ ,  $S_{1:4}$ , and  $S_{1:12}$ , respectively. The initial configurations of the nanorods are cut from a wurtzite crystal. Cutting planes for nanorods expose (0001)<sub>WZ</sub> surfaces and the remaining six side faces are from the  $\{1\bar{2}10\}_{WZ}$ . An example of the nanorod used in the  $S_{1:4}$  simulation is shown embedded in the Lennard-Jones (LJ) pressure medium in Fig. 1.

In MD simulations, a uniform hydrostatic pressure is applied to the nanorods through a liquid medium consisting of atoms interacting via a LJ potential. The LJ potential is parameterized, so that the LJ atoms are in fluid phase at a temperature of  $T=300$  K across a pressure range from  $P=0$  up to  $P=4$  GPa.<sup>19</sup> The CdSe potential consists of two-body and three-body interactions. The fluid-nanorod interaction is modeled by a purely repulsive  $1/r^{12}$  potential.

Simulations are divided into three stages—the initialization stage, where the temperature of the system is raised to 300 K and the pressure correspondingly rise to 180 MPa, the downstroke stage where the pressure is increased to induce the forward transformation, and upstroke at which pressure is decreased and the reverse transformation occurs. The first stage is performed in the microcanonical ensemble (NVE). The second and third stages of the simulation are carried out in the isobaric-isothermal (NPT) ensemble using the Parrinello–Rahman approach.<sup>20</sup>

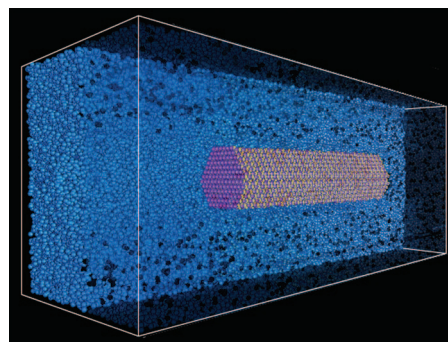


FIG. 1. (Color online) A CdSe nanorod embedded in a Lennard-Jones fluid, which serves as a hydrostatic pressure medium. Each nanorod has a hexagonal cross section, with a diameter of 44 Å. The MD cell cross section for each nanorod is  $165 \text{ Å} \times 165 \text{ Å}$  and lengths are 163, 257, 441, and 1171 Å for  $S_{1:1}$ ,  $S_{1:2}$ ,  $S_{1:4}$ , and  $S_{1:12}$  nanorods, respectively.

<sup>a)</sup>Electronic mail: priyav@usc.edu

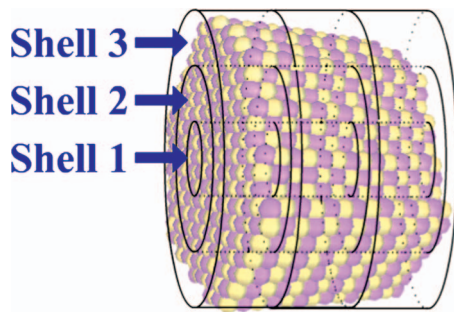


FIG. 2. (Color online) Cylindrical shell-slice analysis. CdSe nanorod is spatially resolved in concentric cylindrical shell slices. Structural quantities are calculated for atoms located in each shell slice, allowing structural differences between different regions within the nanorod to be monitored and compared during the phase transformation.

Spatially resolved calculations of bond-angle distribution and atomic coordination are performed during each simulation. Atoms in each nanorod are divided spatially along its axis into 11-Å “slices” as well as radially into concentric 10 Å-wide “shells” as shown in Fig. 2.

Columns (a) and (b) in Fig. 3 of bond-angle distribution and atomic coordination, respectively. Quantities in rows 1–3 were computed for the nanorods at three different pressures, which we will refer to as the initial, intermediate and final stages of structural transformation. All graphs are color-coded red, blue, and green to correspond to calculations performed in the innermost, middle, and outer shells, respectively. Structural quantities in row 1 show the  $S_{1:1}$  simulation at 180 MPa and 300 K. Here, the bond-angle peak centered about  $109.4^\circ$  in Fig. 3(a1) indicates the nanorod’s initial tetrahedral wurtzite crystal structure. Atomic coordination plots in Fig. 3(b1) show that atoms inside the nanorod have four-

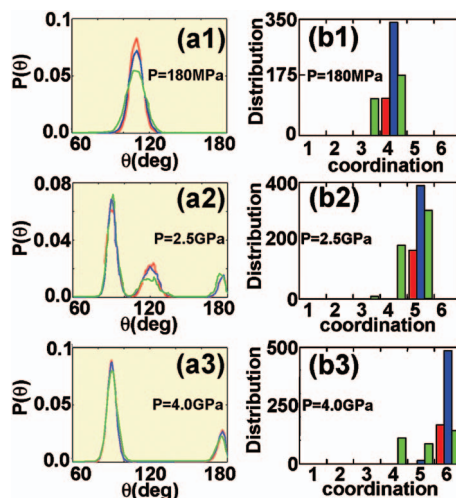


FIG. 3. (Color online) Spatially resolved bond angle [column (a)] and atomic coordination [column (b)] are shown above for the  $S_{1:1}$  nanorod. Red, blue, and green correspond to inner, middle, and outer shells, respectively. Row 1 shows the  $S_{1:1}$  initial configuration at  $T=300$  K,  $P=180$  MPa the nanorod is in the wurtzite phase as indicated by the characteristic bond angle peak centered at  $109.4^\circ$ , and the atomic coordination displaying mostly four-coordinated atoms in every shell. In row 2,  $T=300$  K,  $P=2.5$  GPa, bond angles at  $90^\circ$ ,  $120^\circ$ , and  $180^\circ$  appear, indicating the honeycomb-stacked crystal structure. This is evident from the five-coordinated atoms in all three shells in the corresponding atomic coordination plot. At 4.0 GPa, the crystal phase of the  $S_{1:1}$  nanorod becomes RS as indicated by peaks at  $90^\circ$  and  $180^\circ$  in the bond angles and also by the number of six-coordinated atoms dominating in all shells; see (a3) and (b3).

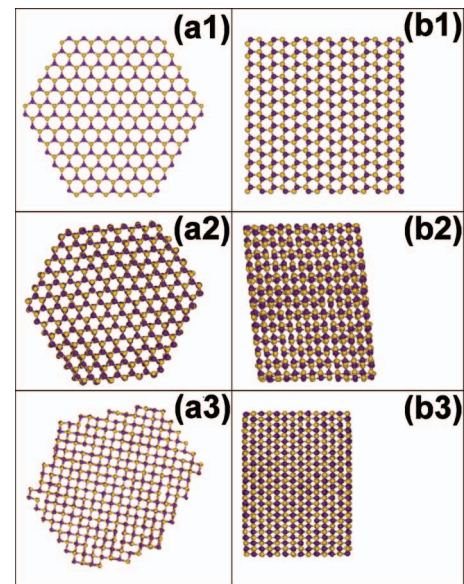


FIG. 4. (Color online) Snapshots of  $S_{1:1}$  nanorod during structural transformation. Columns (a) and (b) show top and side views of the nanorod respectively. Row 1 shows the  $S_{1:1}$  nanorod in pristine wurtzite crystal phase. The honeycombed stacked crystal phase, arising at 1.0 GPa is displayed in row 2. Shearing of atoms in the  $x$ - $y$  plane and contraction of the nanorod along the  $z$  axis ( $\sim 75\%$  compared to the initial) yields the final single crystal rocksalt crystal structure as shown in row 3.

fold coordination, with three-fold and four-fold coordinated atoms at the surface. Shell-resolved bond angle and atomic-coordination distributions for simulations  $S_{1:2}$ ,  $S_{1:4}$ ,  $S_{1:12}$ , at 180 MPa and 300 K are the same as shown for  $S_{1:1}$  in row 1. Row 2 shows structural quantities for the intermediate phase at 2.5 GPa, where the atomic bi-layers in the  $(0001)_{WZ}$  plane of the  $S_{1:1}$  nanorod have flattened under compression along the  $[0001]_{WZ}$  direction into stacked honeycomb lattices, which we refer to as the honeycomb-stacked (HS) structural state. Row 3 shows the structural quantities of the  $S_{1:1}$  system at the final pressure where the crystal structure of the nanorod has transformed to RS. The RS crystal phase is indicated in the bond angle distribution in Fig. 3(a3) by peaks at  $90^\circ$  and  $180^\circ$  deg and by six-coordinated atoms dominating in all three shells in Fig. 3(b3). The structural transformation mechanism we observe is one of several atomic mechanisms described by Shimojo *et al.* in their studies on structural transformations in bulk CdSe using the DFT.<sup>21</sup> They report the WZ-RS-II transition as most favorable, having the lowest energy transition barrier. Final pressures for the nanorods in simulations  $S_{1:1}$ ,  $S_{1:2}$ ,  $S_{1:4}$ , and  $S_{1:12}$ , were  $\sim 4.0$ ,  $\sim 3.0$ ,  $\sim 3.0$ , and  $\sim 2.5$  GPa, respectively.

The final RS phases of the nanorods are highly crystalline. This is apparent in the side and top view images of the  $S_{1:1}$  nanorod in Fig. 4. The structural transition results in a single domain, columns of atoms form periodic arrays from end to end in each nanorod. The cross section of the nanorod has changed shape from its original hexagonal shape, as shown in Fig. 4(a1), to a multidiametered shape shown in Fig. 4(a3). All nanorods also contract during transformation along the  $z$  axis by  $\sim 25\%$ , which is in good agreement with 18% volume contraction observed in experiment on CdSe nanocrystals<sup>22</sup> as well as in the work done in the DFT calculations on CdSe bulk by Shimojo *et al.*, where the lattice constant ratios for the HS and RS phases are 0.813 and 0.707, respectively. By comparing bonding geometries be-

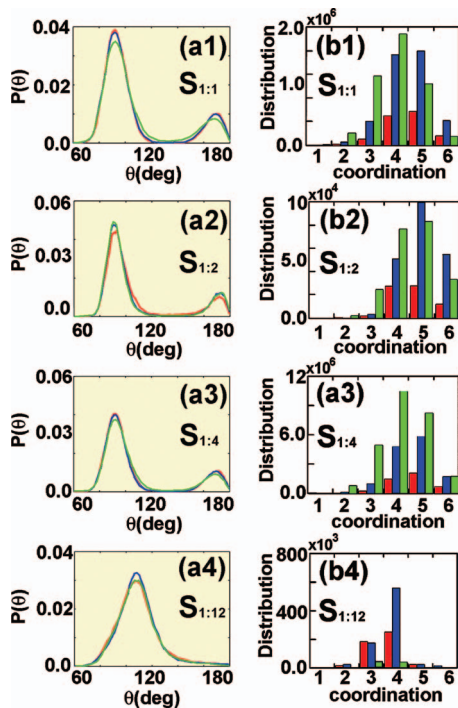


FIG. 5. (Color online) Spatially resolved bond angle distributions [column (a)] and atomic coordinations [column (b)] for the  $S_{1:1}$ ,  $S_{1:2}$ ,  $S_{1:4}$ , and  $S_{1:12}$  nanorod at the end of the upstroke are shown in rows 1–4, respectively. The pressure in all systems shown above is 0.5 MPa. Red, blue, and green correspond to inner, middle, and outer shells, respectively. Peaks at  $90^\circ$  and  $180^\circ$  disappear from all the curves when the atoms at the ends of the nanorod are excluded from shell-resolved bond-angle calculations. Peak at  $109.4^\circ$  in all shells indicates complete reverse transformation to wurtzite begins in the middle of the nanorod and spreads towards the ends.

tween the configurations in Figs. 4(a1) and 4(a3), we also determine that the  $S_{1:1}$  nanorod transforms via the WZ to RS-II mechanism as described by Shimojo *et al.* We also find the nanorods in simulations  $S_{1:2}$ ,  $S_{1:4}$ ,  $S_{1:12}$  to transform by the WZ to RS-II mechanism.

Reverse transformation takes place to the greatest extent in the  $S_{1:12}$  simulation in marked contrast to the smaller nanorods. Structural quantities for the final configuration are shown in Fig. 5. Each row, 1–4 of Fig. 5, shows systems  $S_{1:1}$ ,  $S_{1:2}$ ,  $S_{1:4}$ , and  $S_{1:12}$ , respectively, at the end of the final upstroke stage, after  $\sim 1$  ns simulation time, where the pressure is 0.5 MPa. Comparing Fig. 5 to Fig. 3, broadened peaks in the bond angle distributions and marked shifts in the atomic coordination distributions down from 6 towards 4 in each shell indicate the extent to which reverse structural transformation has proceeded in each system. Bond angle and atomic coordination distributions in system  $S_{1:1}$ ,  $S_{1:2}$ ,  $S_{1:4}$ , shown in rows 1–3, respectively, indicate marginal progress in structural phase transition in comparison to  $S_{1:12}$ . Figure 5(a4) shows peaks in the bond angle distribution centered about  $109^\circ$  clearly visible in all three shells for the  $S_{1:12}$  nanorod at 0.5 MPa. The corresponding atomic coordination distribution in Fig. 5(b4) shows the number of atoms having coordination greater than 4 are negligible in comparison to the number of four-coordinated atoms. The length dependence of structural transformations in the nanorods we have observed can be attributed to surface effects. Shell-resolved analysis reveals that surface atoms are more resistant to

transformation compared to atoms closer to the axis of the nanorods. Thus longer rods, having lower surface-to-volume ratios approaching properties of bulk CdSe, undergo structural transformations more readily compared to shorter nanorods. Surface effects prevail in mitigating crystal phase transformation to a greater extent shorter nanorods as they have higher surface-to-volume ratios.

In conclusion, we have observed a considerable degree of reversibility between structural phases of CdSe nanorods under pressure, with nanorod length shown to be a factor in both forward and reverse structural transformations. Our simulations have shown forward transformation pressure to decrease with increasing nanorod length, which is consistent with experimental observations.<sup>23</sup> Smaller nanoparticles have been reported in experiments to undergo reversible structural transformations with less hysteresis than high-aspect ratio nanorods. In our simulations we see forward and reverse transformation occur more readily in larger nanorods. It should be pointed out that nanorods in experiments are passivated with organic ligands. Nanorod surfaces are not passivated in our simulations. Because surfaces have a strong and direct influence over reverse transformation, surface passivation is an important consideration for future work.

We would like to thank Profs. Paul Alivisatos, Anupam Madhukar and Dr. Gernot Pomrenke for encouragement and support. This work was funded by AFOSR-DURINT, ARO-MURI, DOE, NSF, and DOD Challenge grants. Simulations were performed using resources at the Collaboratory for Advanced Computing and Simulations at USC.

- <sup>1</sup>S. Froyen and M. L. Cohen, Phys. Rev. B **28**, 3258 (1983).
- <sup>2</sup>D. Margetisa, E. Kaxiras, M. Elstner, Th. Frauenheim, and M. R. Manaa, J. Chem. Phys. **117**, 788 (2002).
- <sup>3</sup>E. Kaxiras, Mater. Sci. Forum **232**, 67 (1996).
- <sup>4</sup>M. A. Makeev and A. Madhukar, Phys. Rev. Lett. **86**, 5542 (2001).
- <sup>5</sup>D. Srivastava, M. Menon, C. Daraio, S. Jin, B. Sadanadan, and A. M. Rao, Phys. Rev. B **69**, 153414 (2004).
- <sup>6</sup>B. B. Karki and R. M. Wentzcovitch, Phys. Rev. B **68**, 224304 (2003).
- <sup>7</sup>H. Zhang, B. Gilbert, F. Huang, and J. F. Banfield, Nature (London) **424**, 1025 (2003).
- <sup>8</sup>S. Vemparala, R. K. Kalia, A. Nakano, and P. Vashishta, J. Chem. Phys. **121**, 5427 (2004).
- <sup>9</sup>F. Shimojo, I. Ebbsjö, R. K. Kalia, A. Nakano, J. P. Rino, and P. Vashishta, Phys. Rev. Lett. **84**, 3338 (2000).
- <sup>10</sup>H. Sowa, Z. Kristallogr. **215**, 335 (2000).
- <sup>11</sup>J. N. Wickham, A. B. Herhold, and A. P. Alivisatos, Phys. Rev. Lett. **84**, 923 (2000).
- <sup>12</sup>K. Jacobs, D. Zaziski, E. C. Scher, A. B. Herhold, and A. P. Alivisatos, Science **293**, 1803 (2001).
- <sup>13</sup>D. Zaziski, S. Prilliman, E. C. Scher, M. Casula, J. Wickham, S. M. Clark, and A. P. Alivisatos, Nano Lett. **4**, 943 (2004).
- <sup>14</sup>S. M. Sharma and Y. M. Gupta, Phys. Rev. B **58**, 5964 (1998).
- <sup>15</sup>M. D. Knudson, Y. M. Gupta, and A. B. Kunz, Phys. Rev. B **59**, 11704 (1999).
- <sup>16</sup>S. Limpijumngong and W. R. L. Lambrecht, Phys. Rev. Lett. **86**, 91 (2001).
- <sup>17</sup>H. Sowa, Acta Crystallogr., Sect. A: Found. Crystallogr. **57**, 176 (2001).
- <sup>18</sup>M. Wilson and P. A. Madden, J. Phys.: Condens. Matter **14**, 4629 (2002).
- <sup>19</sup>J. Karl Johnson, J. A. Zollweg, and K. E. Gubbins, Mol. Phys. **78**, 591 (1992).
- <sup>20</sup>M. Parrinello and A. Rahman, Phys. Rev. Lett. **45**, 1196 (1980).
- <sup>21</sup>F. Shimojo, S. Kodiyalam, I. Ebbsjö, R. K. Kalia, A. Nakano, and P. Vashishta, Phys. Rev. B **70**, 184111-1 (2004).
- <sup>22</sup>K. Jacobs, D. Zaziski, E. C. Scher, A. B. Herhold, and A. P. Alivisatos, Science **293**, 1803 (2001).
- <sup>23</sup>S. H. Tolbert, A. B. Herhold, L. E. Brus, and A. P. Alivisatos, Phys. Rev. Lett. **76**, 4384 (1995).